Magnetism in graphene flakes with edge disorder

Sean Deyo [*]
Department of Physics, Cornell University, Ithaca, New York 14853, USA

Selman Hershfield [†]
Department of Physics and National High Magnetic Field Laboratory, University of Florida, Gainesville, Florida 32611, USA

The magnetization of graphene flakes as a function of size, shape, boundary type, and edge defects is computed in a tight-binding model. Flakes with Klein boundaries exhibit a smaller orbital magnetization than flakes with other boundaries. The difference in magnitude is significant for flakes with a few hundred to a few thousand atoms. One can tune the magnetization of a zigzag or Klein flake quasicontinuously by adding atoms, one by one, to the edges of the zigzag flake, or removing atoms from a Klein flake. Flakes with an odd number of atoms show a paramagnetic spin response due to particle-hole symmetry. The addition of a next-nearest neighbor term to the Hamiltonian, which breaks particle-hole symmetry, does not destroy this effect as long as there is approximate particle-hole symmetry. Other defects that affect the chemical potential, such as edge atoms with an onsite potential, or doping, can affect the paramagnetism but preserve the difference in magnetization between Klein and non-Klein flakes. These results are consistent with experiments which see paramagnetic response at low magnetic fields crossing over to diamagnetic response at higher fields.

I. INTRODUCTION

The study of the magnetic properties of graphene and related materials continues to be an active area of investigation. It has long been known that graphite, which has layers of graphene sheets, has a large diamagnetic response [1]. Graphene consists of sp^2 hybridized covalent bonds arranged in a two-dimensional honeycomb lattice. Since each carbon atom in the plane has three nearest neighbors, this leaves one extra electron that does not participate in the covalent bonding. These p$_z$ orbital electrons form a band making graphene a conductor and are responsible for the diamagnetic response, which has been both calculated and observed [2,3].

For any finite sample there are edges to the graphene. The simplest regular edges are the zigzag and armchair edges. It is well established that zigzag edges have a state that is localized near the edge and has energy close to the Fermi energy at half filling, usually referred to as zero energy [4–7]. Armchair edges do not support such an edge state. The edge states for zigzag edges have been observed in STM experiments on the stepped edges of graphite [8–10]. A clear peak in the density of states is seen near zero energy for zigzag edges. Edge states are believed to play an important role in the magnetic response of graphene and graphite [11]. Indeed there are calculations which show that edges can be ferromagnetic and even half metallic [12–14].

Because the coordination number of the carbon atoms at the edges is smaller than that of the atoms in bulk, an edge creates dangling bonds. This makes edges more reactive than the bulk. There is now an extensive literature looking at functionalizing edges of graphene with different types of atoms and molecules [15]. The most common atom to bind to the edge of graphene is hydrogen. This is called hydrogen passivation and has been shown to increase the stability of graphene edges [15–18]. Without hydrogen passivation simulations on small graphene flakes show that the lowest energy state is not always one with a hexagonal pattern [18,19]. Rather there are some atoms near the edge which form pentagons and heptagons. Other types of atoms and molecules are also known to be energetically favorable [20,21] and in some cases lead to local magnetic moments [22]. Another type of edge that has been considered is a single carbon atom, which is then bonded to two hydrogen atoms. An array of such atoms with dihydrogenation is called a Klein edge and has been shown to lead to another type of zero energy edge state [23,24]. Thus, the nature of the edges with defects or reconstruction also influences the magnetism.

There have been a number of experimental reports of ferromagnetism in graphene-related materials [25,26]. Some of these materials have been intentionally damaged by irradiation [27–30] or etching [31]. Others are materials related to graphene like carbon nanocones and nanodisks [32] and graphdiyne [33]. The experimenters do see a small hysteresis in magnetization versus field plots. It is not clear whether this is a phase transition or just a sign of interaction between magnetic moments. At the same time there have been theoretical calculations indicating the possibility for permanent magnetism, such as ferromagnetism, ferrimagnetism, or antiferromagnetism in graphene-derived materials [12–14,34–45]. Some of these calculations rely on

---
[*]sjd257@cornell.edu
[†]selman@phys.ufl.edu

the magnetism of edge states and others on specific kinds of defects.

As indicated above there is always the possibility of defects in any graphene-based small systems because of the edges. Exfoliated nanographite experiments, which aim to reduce the number of impurity atoms to a minimum, have seen a small paramagnetic response at low temperatures in addition to the diamagnetic response [46]. Once the diamagnetic response was subtracted off, the paramagnetic response was found to be isotropic. Other experiments have found a paramagnetic response in graphene-based materials at low temperatures [17,47–52]. Most of these studies intentionally introduce specific impurity atoms on the edges. Thus, there is good evidence for some paramagnetic response in graphene flakes, although it is not clear what the source of the moments is.

In this paper we calculate the magnetic response of small graphene flakes with different types of edge disorder. There have been a number of papers focusing on the magnetic response of small graphene flakes, but previous work has focused on highly regular shapes, largely flakes with triangular or hexagonal shape and edges of one type: either all zigzag or all armchair [53–57]. These papers do see the importance of edge states for the diamagnetic response. Changing the chemical potential to move away from half filling and not include the edge states can change the overall magnetic response from diamagnetic to paramagnetic, although this paramagnetic response does not correspond to a free spin since it cannot be fit to a Brillouin function [57].

The reason for including defects on the edges is that we know they exist from experiment. STM experiments on the edges of graphene show peaks in the density of states near zero energy in small zigzag regions embedded in armchair edges and in other kinds of irregular edges [9,10]. Irregular shapes largely along crystal axes are observed in experiment [46]. There are many cases where specific types of atoms or molecules on edges have been shown to lead to magnetic moments [58–63]. Defects in bulk have also been shown experimentally [51,52,64,65] and theoretically [52,66–69] to lead to magnetic moment formation, although we do not consider those here.

The model we use is the conventional tight-binding model for graphene. This has been shown to describe edge states well [70]. There are interacting models of the edges that show ferromagnetism and other types of magnetic order at the edges [12–14,44], which our model does not include. At the end of the paper we discuss the relation of our results to experiment and to the predictions of these interacting models. We first consider different shapes and sizes of graphene flakes, including flakes with mixtures of zigzag and armchair edges. These correspond to graphene edges which have hydrogen terminations to stabilize the edge structure. We next move on to considering single defects on the edges such as an edge with an extra carbon atom or an edge missing a few carbon atoms. For these defects we are able to understand under what conditions a paramagnetic response is seen. Thus, while our tight-binding model is simple, the understanding allows one to see the range of possible magnetic responses and under what conditions they may arise. This is particularly useful because for a given experiment one usually does not know the

actual configuration of impurities or the exact structure of the edge.

We compute both the orbital and spin contributions of the magnetic susceptibility. As seen in many experiments, we find a paramagnetic response visible at low temperatures superimposed on a diamagnetic response. The edge disorder affects both the diamagnetic and paramagnetic response. Our model does not include interactions so we can not see any vestiges of ferromagnetic or spin glass behavior. However, this noninteracting model would form the starting point for distinguishing in experiments between noninteracting and interaction effects and in building a full model to include both disorder and interactions.

The rest of the paper is organized as follows. In the next section we describe the equations which we solve numerically to find the magnetization and susceptibility. In Sec. III we present results and discussion for the magnetization for regularly shaped graphene flakes and flakes with defects along their edges. Conclusions are given in Sec. IV.

II. MODEL

The nearest-neighbor tight-binding Hamiltonian for graphene is

$$H = -\gamma \sum_{(m,n),s} e^{i\phi_{m,n}} c^{\dagger}_{m,s} c_{n,s} + g\mu_B B \sum_{n,s} s \, c^{\dagger}_{n,s} c_{n,s}, \quad (1)$$

where $g = 2$ and μ_B is the Bohr magneton. The summation variables m and n represent sites in the two-dimensional honeycomb lattice of graphene, with the parentheses indicating that the first sum is over nearest neighbor pairs. We assume the graphene sheet is in the x-y plane and let s be the spin quantum number in the z direction, summing over $s = \pm 1/2$. The hopping parameter γ can be obtained by fitting to first principles band structure calculations [71] with values ranging between 2.5 and 3.0 eV. We will use a value of 2.8 eV. Next-nearest-neighbor hopping, which is known to break particle-hole symmetry, will be included later in Sec. III C to test for the robustness of the effects observed. The orbital contribution of magnetic field is included via the Peierls phase factor,

$$\phi_{m,n} = \frac{e}{\hbar} \int_{r_m}^{r_n} \vec{A} \cdot \vec{r}'. \quad (2)$$

Here r_m and r_n are the positions of the m and n sites, and $e = |e|$ is the magnitude of the charge of an electron.

The magnetization is the derivative of the free energy with respect to the magnetic field B:

$$M = -\frac{\partial \Omega}{\partial B}. \quad (3)$$

The free energy in the grand canonical ensemble is

$$\Omega = -k_B T \sum_{\alpha,s} \ln(1 + e^{-\beta(\epsilon_{\alpha,s} - \mu)}), \quad (4)$$

where $\beta = 1/k_B T$ and $\epsilon_{\alpha,s}$ are the energy eigenvalues obtained by diagonalizing the Hamiltonian in Eq. (1). The grand canonical ensemble is used as a calculational technique. We find that the number of electrons is constant to a high degree in all cases except when we move away from half filling, in which case it varies slightly, so these results apply equally

well to the canonical ensemble. Taking the derivative of this with respect to B the magnetization is

$$M = -\sum_{\alpha,s} \frac{1}{1 + e^{\beta(\epsilon_{\alpha,s}-\mu)}} \frac{\partial \epsilon_{\alpha,s}}{\partial B}. \tag{5}$$

There are two contributions to the energy and the magnetization, one from the orbital motion and one from the spin degree of freedom. In the absence of spin-orbit coupling these are independent. Rather than take the derivative of the energy numerically one can use first-order perturbation theory to take the derivative analytically. The result can be expressed in a fashion that is numerically efficient and makes connection to a classical expression for the magnetization. It is written in terms of the current operator I from site r_m to r_n:

$$I(r_m \rightarrow r_n) = \frac{ie}{\hbar} \gamma \sum_s \{e^{i\phi_{m,n}} c_{m,s}^\dagger c_{n,s} - \text{H.c.}\}. \tag{6}$$

With this operator the orbital part of the magnetization is

$$M_{\text{orb}} = \frac{1}{4} \sum_{(m,n)} \langle I(r_m \rightarrow r_n)\rangle (\vec{r}_m \times \vec{r}_n)_z. \tag{7}$$

The angular brackets around the current operator I denote a thermal average. The summand in Eq. (7) is even under the interchange $m \leftrightarrow n$. One can show that this expression for the magnetization is gauge invariant using the continuity equation for the density.

The energy derivative for the spin component is $g\mu_B s$ so the spin contribution to the magnetization is

$$M_{\text{spin}} = \sum_{\alpha,s} -g\mu_B s \frac{1}{1 + e^{\beta(\epsilon_{\alpha,s}-\mu)}}. \tag{8}$$

In the following we diagonalize the Hamiltonian, Eq. (1), for a given lattice and applied magnetic field. We then apply Eqs. (7) and (8) to compute the magnetization as a function of magnetic field and temperature.

The orbital diamagnetic response will be linear for most experimentally accessible field scales, so we can express the orbital response in terms of the susceptibility, which we define as $\chi = \partial M/\partial B$. The natural scale for the susceptibility is $\chi_o = \gamma e^2 a^4/\hbar^2 = 2.63 \times 10^{-9}$ eV/T^2, where $\gamma = 2.8$ eV is the nearest-neighbor hopping energy and $a = 1.42$ Å is the distance between neighboring atoms. The scale of the magnetization used for the spin and total magnetic response is set by the Bohr magneton μ_B. Finally, in describing the size of our flakes, we will use the circumradius R, which is simply the radius of the smallest circle that encloses the flake.

III. RESULTS & DISCUSSION

A. Ordered boundaries and shapes

We begin by considering the four different ordered boundary types of hexagonal flake depicted in Fig. 1: (a) armchair with peninsular corners, (b) armchair with rounded corners, (c) zigzag, and (d) Klein. These ordered cases will act as a reference and motivate the disordered edges considered later. Both zigzag and armchair edges are seen in STM images of edges in graphene. In practice they can be realized by
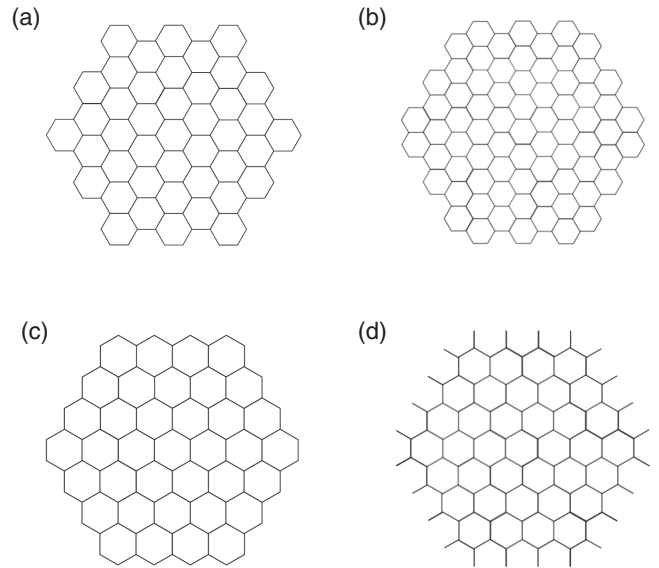

FIG. 1. Illustration of the four types of ordered boundaries considered: (a) armchair with peninsular corners, (b) armchair with rounded corners, (c) zigzag, and (d) Klein.

hydrogenating the extra carbon bond at the edge. A Klein edge has two extra carbon bonds so it needs two hydrogen atoms per carbon edge atom to stabilize.

The orbital susceptibility as a function of circumradius for the four different boundary types of hexagonal flakes is shown in Fig. 2. The armchair and zigzag flakes have similar magnitudes for their orbital susceptibilities, whereas those of the Klein flakes are markedly smaller. The only difference between the zigzag and the Klein flakes is their boundaries. While one might expect a large difference based on the boundary type for small flakes, this difference persists even for larger flakes. We will have an extensive discussion including the spin component of the magnetization once we consider single defects along the edge, but for now we only consider the orbital response.
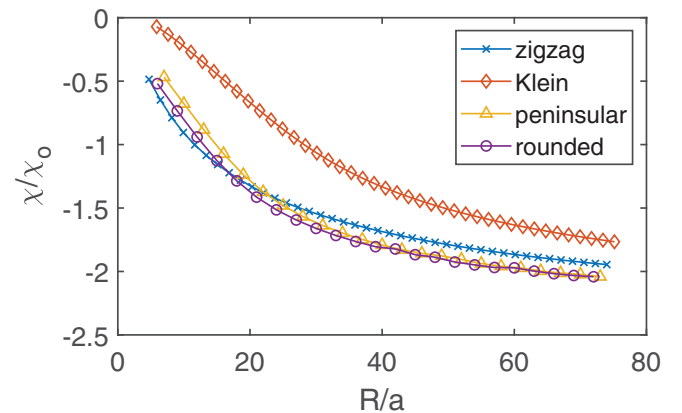

FIG. 2. Orbital susceptibility vs circumradius for hexagonal flakes with four different types of boundaries at zero temperature. The scale χ_o is $\gamma e^2 a^4/\hbar^2$, where γ is the tight-binding hopping and a is the nearest-neighbor distance.
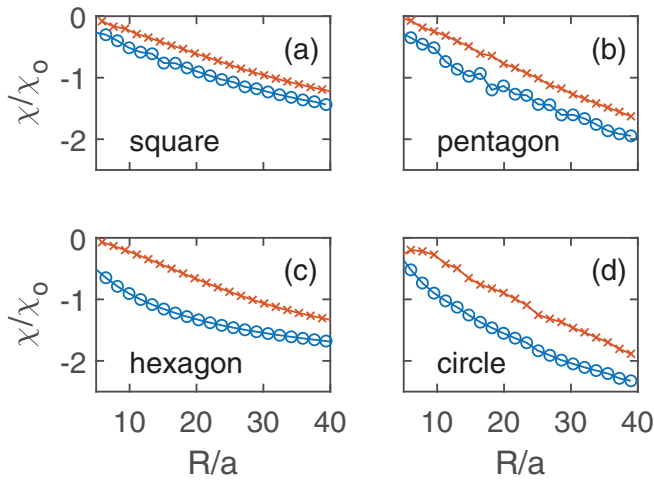
FIG. 3. Orbital susceptibility vs circumradius for various shapes at zero temperature, comparing Klein and non-Klein boundaries. The blue circles are for the non-Klein boundaries, and the red x's are for the Klein boundaries. In all cases the susceptibility for the Klein boundaries is substantially smaller in magnitude than for the non-Klein boundaries.

The only regular polygons that fully respect the symmetry of graphene's lattice are the hexagon and the triangle. However, we can still investigate the Klein vs non-Klein phenomenon for other shapes. To ensure a flake has no Klein boundaries, one can remove all carbon atoms with only one nearest neighbor; likewise, to maximize Klein boundaries, one can remove all carbon atoms with two nearest neighbors. This latter method requires at least some portion of the flake's boundary to be of the zigzag type, since an armchair boundary cannot be made Klein in this fashion. Arbitrary flakes generally have a mix of armchair and zigzag/Klein boundaries, so the comparison is not as stark for shapes without trigonal symmetry.

Nonetheless, we can make an analog of Fig. 2 for other shapes. This is given in Fig. 3. We do not distinguish between armchair and zigzag boundary types, since both are present in flakes that lack trigonal symmetry, but we can still distinguish between maximum Klein and no Klein, as described above. The difference in magnitude between the two is clear, albeit smaller than it was for the hexagons. Shape does indeed affect the susceptibility; however, non-Klein boundaries produce greater susceptibility than Klein ones regardless of shape.

The difference between the Klein edges and the other edges raises the question of whether the orbital susceptibility could somehow be tuned between the two extremes. To answer this question, we begin with a zigzag flake and randomly add atoms to the boundary, one at a time, to gradually convert it to a Klein flake. At each step we compute the magnetic response. One can also add atoms in order, picking a starting point and following the boundary in, say, the clockwise direction. Figure 4 shows the change in orbital susceptibility, one atom at a time, for both the random and the orderly methods starting with a hexagonal zigzag flake of circumradius $14a/\sqrt{3}$. One can see that the change is steeper for the first few atoms added than for the last few atoms. The orderly method exhibits six cycles of a steeper change followed by a brief respite,
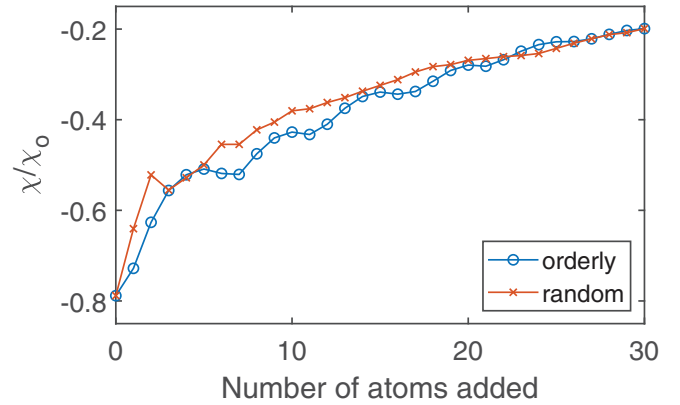

FIG. 4. Orbital susceptibility vs number of atoms added to the boundary for a hexagonal zigzag flake, with the atoms added either randomly or sequentially.

corresponding to each side of the hexagon being altered. Apart from this phenomenon, the change is almost monotonic for both methods. In short, the answer appears to be yes, one can tune the response quasicontinuously between the Klein and non-Klein by adding (or removing) an appropriate number of boundary atoms, and the order in which atoms are added does not drastically affect the tuning process.

B. Defects

Because there is a substantial change in the magnetic response for only a single defect, as seen in Fig. 4, we next consider single localized defects on otherwise perfectly ordered zigzag and armchair flakes. Here we consider the total magnetization, including both the orbital and spin contributions. For the previous flakes with perfect zigzag and armchair edges the spin contribution was not important. Here it will be. We have considered a large number of different possible defect configurations. In Fig. 5 we show four of them: (a) a zigzag edge with an extra atom, (b) a zigzag edge missing an atom, (c) an armchair edge with an extra atom, and (d) an armchair edge missing two atoms. We have also considered multiple extra atoms and flakes with mixtures of armchair and zigzag edges. These are not localized defects. However, we can understand all cases by first understanding the four cases shown in Fig. 5. In the following plots we will keep the same order (a)–(d) for these results so, for example, (a) always refers to the zigzag case with an extra atom.

In Fig. 6 the magnetization due to both spin and orbital contributions is shown for a magnetic field perpendicular to the flakes. There is a strong paramagnetic response for cases (a)–(c) at lower temperatures, gradually transitioning to a diamagnetic response as the temperature is increased. Only case (d), which is the armchair hexagon with two missing sites, shows no paramagnetic response. For comparison, the dashed black line in this figure is the magnetic response for the corresponding flake without a defect—that is, the zigzag or armchair magnetic response examined in the previous subsection. As noted in the introduction, behavior like this has been observed experimentally, including in experiments which have sought to minimize defects. It is well know that zigzag edges support edge states while armchair edges do not;
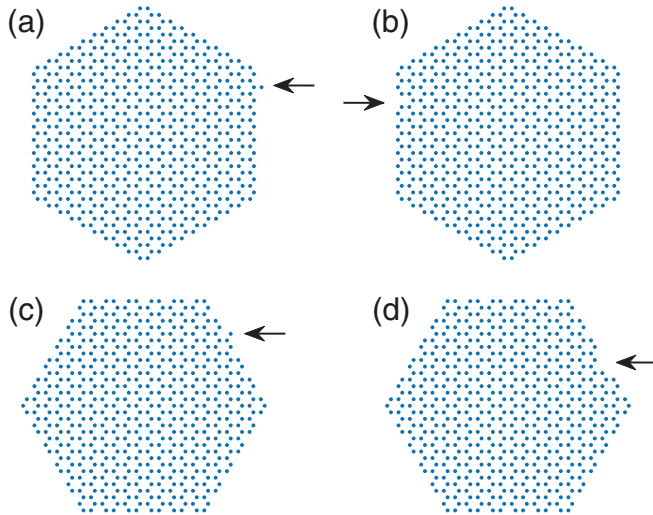
FIG. 5. Different types of defects. These are representative types of surface defects that we have considered. (a) Zigzag flake with an extra atom on the edge. (b) Zigzag flake missing an atom on the edge. (c) Armchair flake with an extra atom. (d) Armchair flake missing two atoms. Cases (a)–(c) have an odd number of sites, while case (d) has an even number of sites. In the following figures (a)–(d) will refer to these cases.

FIG. 7. Energy versus state index for states near zero energy. For cases (a), (b), (c) there is a state exactly at zero energy, which is required by symmetry if there is an odd number of sites. Case (d) with an even number of sites does not have a state at zero energy.

however, the difference between case (d) and the other three cases is not the difference between zigzag and armchair edges because case (c) is based on an armchair edge.

The key difference between case (d) and the other cases can be seen by looking at the energies of the states near zero energy. Graphene with nearest-neighbor hopping is a bipartite lattice with an energy spectrum which is symmetric about $E = 0$ due to particle-hole symmetry. In Fig. 7 we plot the

energy of the orbital states near zero energy for the same four cases. The indices are those of the states with 1 being the lowest-energy state. One can see that in cases (a)–(c) there is a state exactly at $E = 0$. With an odd number of sites, and thus an odd number of orbital states, there must be an odd number of states at zero energy because of the symmetry about $E = 0$. In particular, there must be at least one state at zero energy. That state is the source of the paramagnetic response. It behaves within this noninteracting model as a spin 1/2 defect. On the other hand, case (d) has an even number of sites, so the symmetry about $E = 0$ requires that there be an even number of states at zero energy. In particular, zero states is a possibility. Since there is no state at zero energy for case (d), there is no paramagnetic response. These results are consistent with the more general theorem of Lieb for the case of repulsive Hubbard U interactions on an unbalanced bipartite lattice [72].

We have found some cases with an even number of sites where there are two states very nearly at zero energy, but that is a coincidence and not required by symmetry. The difference between an even and odd number of sites is the key difference between paramagnetic and nonparamagnetic response. All flakes show diamagnetic response at large magnetic fields. Thus, if one has a number of defects along the edges, perhaps of different types, paramagnetic response is determined by whether there is an even or odd number of states on the flake.

A key fact here is that the flakes are at half filling. While we work in the grand canonical ensemble, which does not fix the number of electrons, we have checked our calculation in the temperature and field regime shown in the figures and find that the variation in the number of electrons is negligible. For example in a flake with 601 sites the number of electrons calculated in the grand canonical ensemble is 601 ± 10^{-8} for plots like those in the figures. This extremely small variation is due to the density of states being symmetric about the Dirac point.
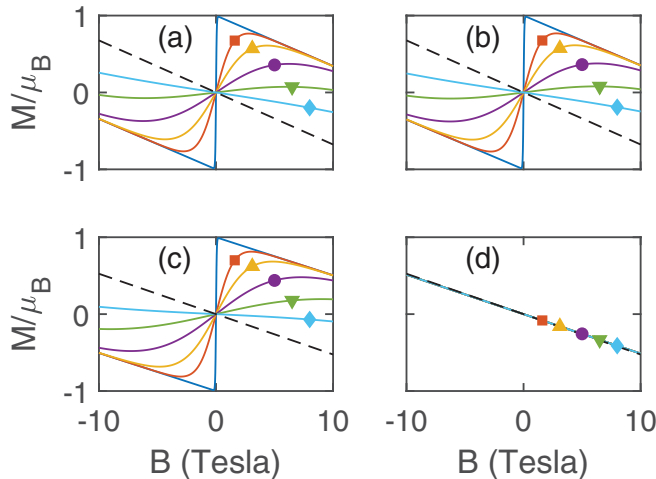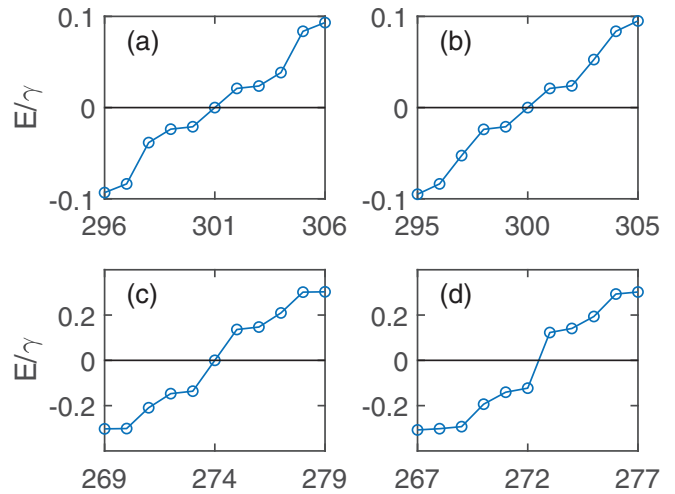

FIG. 6. Magnetization due to both spin and orbital contributions for a magnetic field perpendicular to the flakes. The cases (a)–(d) are the same as in the previous figure. The colors refer to different temperatures $T = 0.02$ K (blue line), 0.52 K (orange, ■), 1.02 K (yellow, ▲), 2.02 K (purple, ●), 4.02 K (green, ▼), 8.02 K (light blue, ♦). All the temperature curves overlap for case (d). For comparison the black dashed line is the magnetic response for a zigzag flake, (a) and (b), or armchair flake, (c) and (d), without a defect.
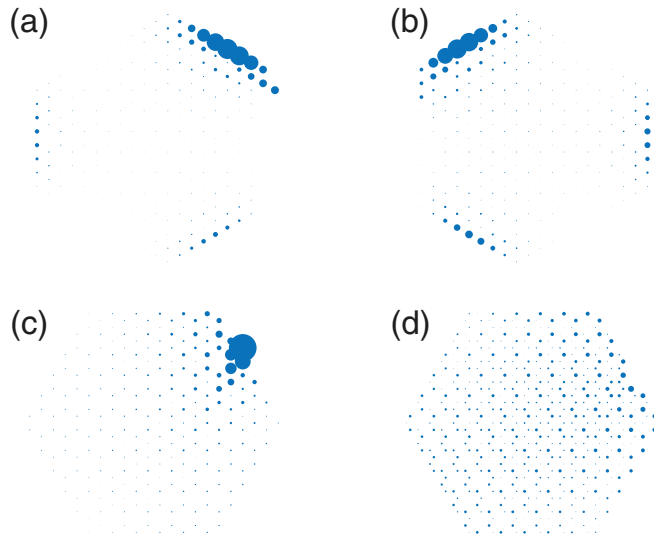
FIG. 8. Visualization of the state closest to zero energy. The area of the circles is proportional to the wave function squared at a given site. The cases (a)–(d) are the same as in the previous figures.

FIG. 9. Magnetization in the presence of next-nearest neighbor hopping. Colors and labels are the same as for Fig. 6.

To visualize the states responsible for the paramagnetic response we have plotted in Fig. 8 the states closest to zero energy. For cases (a)–(c) this is a state at zero energy, while for case (d) it is the state closest to zero energy. The area of the circle plotted at each site is proportional to the magnitude squared of the wave function. Thus, a state which is localized on a few sites shows up as a few large circles, while an extended state consists of many small circles. The zero-energy states for the zigzag hexagons, cases (a) and (b), are localized along the edges. This shows strong hybridization of the edge state with the defect. In fact, by comparing Figs. 5 and 8 one can see there is actually a greater probability that the electron will be on an edge adjacent to the defect than on the edge containing the defect. Armchair edges do not support edge states like zigzag edges do, so their zero-energy states are not spread along edges: In case (c) the zero-energy state is localized just around the defect, not the entire edge; in case (d), the flake that had no paramagnetic response and no zero-energy state, the state closest to zero energy is extended throughout the lattice, despite a slight bias toward the edge where the defect lies.

C. Particle-hole symmetry broken

The particle-hole symmetry about $E = 0$ is broken once one includes next-nearest neighbor hopping. The next-nearest neighbor hopping is much smaller than the nearest-neighbor hopping in graphene, but is nonetheless nonzero. In Fig. 9 we show the magnetic response for the same cases but with a next-nearest neighbor hopping of 0.28 eV, which is one tenth the magnitude of the nearest-neighbor hopping of $\gamma = 2.8$ eV. The plots are very nearly the same as in Fig. 6 with one fine point: Turning on next-nearest neighbor interactions shifts all the energies. The half-filling point is no longer at zero energy. Thus, in these plots we have placed the chemical potential at half filling. For an odd number of atoms or sites this means that there is at least one state right at the chemical
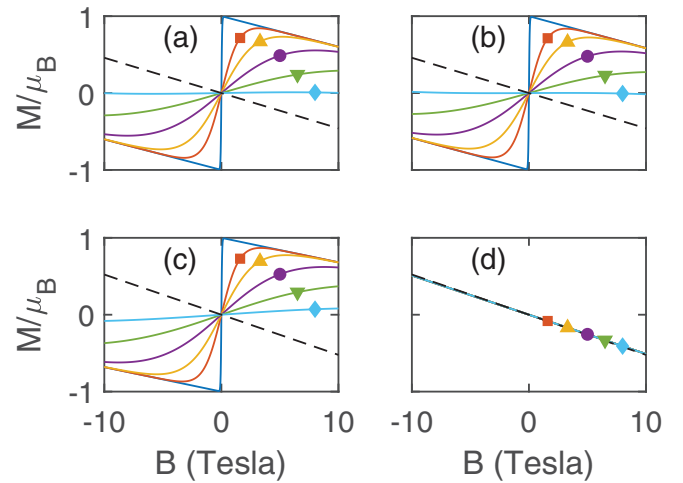
potential. For an even number of sites, we place the chemical potential between the middle two energy eigenstates, so there is no state at the chemical potential unless the middle two eigenstates are degenerate. The important point is that next-nearest neighbor hopping does not destroy the effect described in the previous subsection. It breaks particle-hole symmetry, but the primary consequence is just an overall energy shift that varies weakly from one state to the next. For this case as for the particle-hole symmetric case the number of electrons calculated is constant for the field and temperature scale in the figures.

Another way to break the particle-hole symmetry is to have an onsite potential for the edge defect. Even if the edge defect is a dihydrogenated carbon, the effective onsite potential will not be zero. The contribution to the spin magnetization for a state with energy E is

$$
\mu_B \left\{ \frac{1}{e^{\beta(E - \mu_B B - \mu)} + 1} - \frac{1}{e^{\beta(E + \mu_B B - \mu)} + 1} \right\}
$$
$$
= \frac{\mu_B}{2} \left\{ \tanh \frac{\mu_B B - E + \mu}{2 k_B T} + \tanh \frac{\mu_B B + E - \mu}{2 k_B T} \right\}. \quad (9)
$$

As $|E - \mu|$ becomes larger the two tanh functions begin to separate and eventually there is no longer a paramagnetic response. In Fig. 10 the spin magnetic response as a function of magnetic field is shown for a zigzag flake with a defect that has a nonzero onsite energy (black x's). An energy at the site of the defect of $\epsilon_o = 0.014$ eV produces an energy shift of $E = 1.12 \times 10^{-4}$ eV. The ordinary spin 1/2 Brillouin function is starting to split into two different step functions. The solid line is the fit to Eq. (9). The reason the energy shift is so much smaller than the onsite potential is that the states near zero energy are extended around the edge of the flake. The weight of the wave function at the defect site is $|\psi|^2 = 0.008$. Thus, according to first order perturbation theory the energy shift is $\epsilon_o |\psi|^2$, which is indeed 1.12×10^{-4} eV. Note that the armchair defect states are much more localized with a weight at the defect site of $|\psi|^2 = 0.4$. Thus, even a very small potential on a defect on an armchair edge is likely to move it
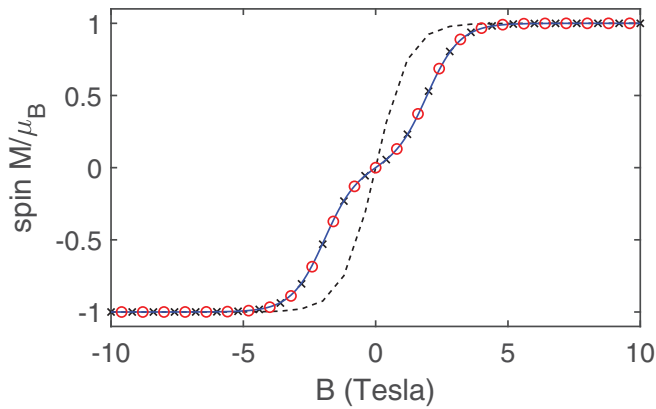
FIG. 10. Effect on the spin component of the magnetization due to a nonzero chemical potential or a nonzero defect energy. The red circles are for a chemical potential of 1.12×10^{-4} eV. The black x's are for an onsite defect potential of 0.014 eV, which produces an energy shift of 1.12×10^{-4} eV. The solid blue line is for Eq. (9) with the same parameters. The dashed line is for Eq. (9) with the chemical potential shifted to ensure half filling; that is, $\mu = E$. The temperature is 0.42 K.

substantially away from zero energy. For this reason we expect the paramagnetic response to be more robust for zigzag edges.

The orbital magnetization is not shown in the figure because for this onsite potential the diamagnetic response remains linear and changes much less than one percent. The spin response is more sensitive to a local potential at the defect. As indicated earlier the orbital magnetization is sensitive to the existence of defects or a Klein edge, but adding this size potential has very little effect on the diamagnetic susceptibility.

We note that, unlike the cases in Sec. III B, the number of electrons does vary here. If one shifts the chemical potential so as to remain at half filling in the presence of an onsite potential, the spin paramagnetism is preserved. This is shown as the dashed line in Fig. 10. Thus, the paramagnetic effect is more robust when the number of electrons is fixed. However, if one introduces doping instead of an onsite potential, half filling no longer applies. This is illustrated in Fig. 10 by the red circles which correspond to a chemical potential of $\mu = 1.12 \times 10^{-4}$ eV. Shifting μ while keeping E fixed has the same effect as shifting E while keeping μ fixed.

IV. CONCLUSIONS

In this paper we have computed the magnetic response in graphene flakes with different shapes and edges, including defects along the edges. While the orbital magnetic response does depend on the size and shape of the flake, we found the largest effect to be the reduction in the orbital diamagnetic response for Klein edges as opposed to armchair, zigzag, or

some combination thereof. Even a few defects of the kind present in a Klein edge can lead to a substantial reduction in the diamagnetic response.

Many different kinds of defects can induce a paramagnetic response. We have considered flakes with single or multiple defects, zigzag or armchair edges, or mixtures of zigzag and armchair edges along with multiple defects. However, all cases can be understood from the four representative examples we have shown—adding a single atom along the edge or taking away one or two atoms along the edge for zigzag and armchair hexagons. The origin of the effect here is zero-energy states or, more generally, states at the chemical potential. Such states must exist in a system with an odd number of sites and particle-hole symmetry or near particle-hole symmetry. They can also occur for an even number of states but are not required by symmetry. The states near zero energy are extended along the edge for zigzag edges indicating strong hybridization with the edge states. On the other hand the zero-energy states are localized on the defect for an armchair flake because armchair flakes do not support edge states. Consequently, the paramagnetic response in zigzag flakes is more robust to perturbations by a local onsite potential. The effect is also more robust for isolated flakes where the number of electrons is constant at half filling, although doping could remove the half filling requirement and disrupt the paramagnetic response.

Parts of these results are consistent with experiments such as Ref. [46], which tries to examine the intrinsic magnetism in graphene flakes. The experiments would suggest a magnetic moment of at most a few μ_B per flake. Roughness would increase the number of moments without the need for special impurities. As noted in the introduction there are a number of calculations that show ferromagnetism, particularly for zigzag edges in nanoribbons. If each zigzag edge is ferromagnetic or superparamagnetic, then the response would be much larger than what is observed [46]. On the other hand, if the curved nature of flakes means that some of the ferromagnetic response is destroyed, that could either account for the magnetization observed directly or in coupling with the effect studied here by enhancing the paramagnetic spin response. Interactions between moments on different flakes could also produce a larger effective moment. The calculated field dependence here is that of a spin 1/2 impurity, not the higher spin seen in many experiments, but it is an open question what happens when one includes interactions between the spins of these defects and other possible interaction effects.

[1] K. Krishnan, Magnetic anisotropy of graphite, Nature (London) **133**, 174 (1934).

[2] J. McClure, Diamagnetism of graphite, Phys. Rev. **104**, 666 (1956).

[3] A. H. Castro Neto, F. Guinea, N. M. R. Peres, K. S. Novoselov, and A. K. Geim, The electronic properties of graphene, Rev. Mod. Phys. **81**, 109 (2009).

[4] M. Fujita, K. Wakabayashi, K. Nakada, and K. Kusakabe, Peculiar localized state at zigzag graphite edge, J. Phys. Soc. Jpn. **65**, 1920 (1996).

[5] P. Potasz, A. D. Güçlü, and P. Hawrylak, Zero-energy states in triangular and trapezoidal graphene structures, Phys. Rev. B **81**, 033403 (2010).

[6] M. Ezawa, Dirac fermions in a graphene nanodisk and a graphene corner: Texture of vortices with an unusual winding number, Phys. Rev. B **81**, 201402(R) (2010).

[7] M. Zarenia, A. Chaves, G. A. Farias, and F. M. Peeters, Energy levels of triangular and hexagonal graphene quantum dots: A comparative study between the tight-binding and dirac equation approach, Phys. Rev. B **84**, 245403 (2011).

[8] Y. Niimi, T. Matsui, H. Kambara, K. Tagami, M. Tsukada, and H. Fukuyama, Scanning tunneling microscopy and spectroscopy studies of graphite edges, Appl. Surf. Sci. **241**, 43 (2005).

[9] Y. Kobayashi, K.-i. Fukui, T. Enoki, K. Kusakabe, and Y. Kaburagi, Observation of zigzag and armchair edges of graphite using scanning tunneling microscopy and spectroscopy, Phys. Rev. B **71**, 193406 (2005).

[10] Y. Kobayashi, K.-i. Fukui, T. Enoki, and K. Kusakabe, Edge state on hydrogen-terminated graphite edges investigated by scanning tunneling microscopy, Phys. Rev. B **73**, 125415 (2006).

[11] K. Wakabayashi, M. Fujita, H. Ajiki, and M. Sigrist, Electronic and magnetic properties of nanographite ribbons, Phys. Rev. B **59**, 8271 (1999).

[12] Y.-W. Son, M. L. Cohen, and S. G. Louie, Energy Gaps in Graphene Nanoribbons, Phys. Rev. Lett. **97**, 216803 (2006).

[13] Y.-W. Son, M. L. Cohen, and S. G. Louie, Half-metallic graphene nanoribbons, Nature (London) **444**, 347 (2006).

[14] G. Cantele, Y.-S. Lee, D. Ninno, and N. Marzari, Spin channels in functionalized graphene nanoribbons, Nano Lett. **9**, 3425 (2009).

[15] A. Bellunato, H. Arjmandi Tash, Y. Cesa, and G. F. Schneider, Chemistry at the edge of graphene, ChemPhysChem **17**, 785 (2016).

[16] Y. Miyamoto, K. Nakada, and M. Fujita, First-principles study of edge states of h-terminated graphitic ribbons, Phys. Rev. B **59**, 9858 (1999).

[17] L. Song, X. Zheng, R. Wang, and Z. Zeng, Dangling bond states, edge magnetism, and edge reconstruction in pristine and b/n-terminated zigzag graphene nanoribbons, J. Phys. Chem. C **114**, 12145 (2010).

[18] D. P. Kosimov, A. A. Dzhurakhalov, and F. M. Peeters, Carbon clusters: From ring structures to nanographene, Phys. Rev. B **81**, 195414 (2010).

[19] O. Voznyy, A. D. Güçlü, P. Potasz, and P. Hawrylak, Effect of edge reconstruction and passivation on zero-energy states and magnetism in triangular graphene quantum dots with zigzag edges, Phys. Rev. B **83**, 165417 (2011).

[20] R. Saito, M. Yagi, T. Kimura, G. Dresselhaus, and M. Dresselhaus, Electronic structure of fluorine doped graphite nanoclusters, J. Phys. Chem. Solids **60**, 715 (1999).

[21] M. Zhao, F. Yang, Y. Xue, D. Xiao, and Y. Guo, Effects of edge oxidation on the stability and half-metallicity of graphene quantum dots, ChemPhysChem **15**, 157 (2014).

[22] M. Maruyama and K. Kusakabe, Theoretical prediction of synthesis methods to create magnetic nanographite, J. Phys. Soc. Jpn. **73**, 656 (2004).

[23] D. Klein, Graphitic polymer strips with edge states, Chem. Phys. Lett. **217**, 261 (1994).

[24] D. Klein and L. Bytautas, Graphitic edges and unpaired π-electron spins, J. Phys. Chem. A **103**, 5196 (1999).

[25] P. Esquinazi, A. Setzer, R. Höhne, C. Semmelhack, Y. Kopelevich, D. Spemann, T. Butz, B. Kohlstrunk, and M. Lösche, Ferromagnetism in oriented graphite samples, Phys. Rev. B **66**, 024429 (2002).

[26] W. L. Wang, S. Meng, and E. Kaxiras, Graphene nanoflakes with large spin, Nano Lett. **8**, 241 (2008).

[27] A. V. Rode, E. G. Gamaly, A. G. Christy, J. G. Fitz Gerald, S. T. Hyde, R. G. Elliman, B. Luther-Davies, A. I. Veinger, J. Androulakis, and J. Giapintzakis, Unconventional magnetism in all-carbon nanofoam, Phys. Rev. B **70**, 054407 (2004).

[28] P. Esquinazi, D. Spemann, R. Höhne, A. Setzer, K.-H. Han, and T. Butz, Induced Magnetic Ordering by Proton Irradiation in Graphite, Phys. Rev. Lett. **91**, 227201 (2003).

[29] S. Talapatra, P. G. Ganesan, T. Kim, R. Vajtai, M. Huang, M. Shima, G. Ramanath, D. Srivastava, S. C. Deevi, and P. M. Ajayan, Irradiation-Induced Magnetism in Carbon Nanostructures, Phys. Rev. Lett. **95**, 097201 (2005).

[30] H. Ohldag, T. Tyliszczak, R. Höhne, D. Spemann, P. Esquinazi, M. Ungureanu, and T. Butz, π-Electron Ferromagnetism in Metal-Free Carbon Probed by Soft X-Ray Dichroism, Phys. Rev. Lett. **98**, 187204 (2007).

[31] N. Soin, S. C. Ray, S. Sarma, D. Mazumder, S. Sharma, Y.-F. Wang, W.-F. Pong, S. S. Roy, and A. M. Strydom, Tuning the electronic and magnetic properties of nitrogen-functionalized few-layered graphene nanoflakes, J. Phys. Chem. C **121**, 14073 (2017).

[32] J. Černák, G. Helgesen, E. Čižmár, J. Kováč, Z. Jurašeková, and J. Voltr, Magnetic properties of graphene nanodisk and nanocone powders at low temperatures, Phys. Rev. B **92**, 155429 (2015).

[33] Y. Zheng, Y. Chen, L. Lin, Y. Sun, H. Liu, Y. Li, Y. Du, and N. Tang, Intrinsic magnetism of graphdiyne, Appl. Phys. Lett. **111**, 033101 (2017).

[34] K. Harigaya and T. Enoki, Mechanism of magnetism in stacked nanographite with open shell electrons, Chem. Phys. Lett. **351**, 128 (2002).

[35] K. Kusakabe and M. Maruyama, Magnetic nanographite, Phys. Rev. B **67**, 092406 (2003).

[36] H. Kumazaki and D. S. Hirashima, Nonmagnetic-defect-induced magnetism in graphene, J. Phys. Soc. Jpn. **76**, 064713 (2007).

[37] J. Fernández-Rossier and J. J. Palacios, Magnetism in Graphene Nanoislands, Phys. Rev. Lett. **99**, 177204 (2007).

[38] O. V. Yazyev, Magnetism in Disordered Graphene and Irradiated Graphite, Phys. Rev. Lett. **101**, 037203 (2008).

[39] O. V. Yazyev, Emergence of magnetism in graphene materials and nanostructures, Rep. Prog. Phys. **73**, 056501 (2010).

[40] R. Faccio, H. Pardo, P. A. Denis, R. Y. Oeiras, F. M. Araújo-Moreira, M. Veríssimo-Alves, and A. W. Mombrú, Magnetism induced by single carbon vacancies in a three-dimensional graphitic network, Phys. Rev. B **77**, 035416 (2008).

[41] B. Wunsch, T. Stauber, F. Sols, and F. Guinea, Interactions and Magnetism in Graphene Boundary States, Phys. Rev. Lett. **101**, 036803 (2008).

[42] T. Enoki and K. Takai, The edge state of nanographene and the magnetism of the edge-state spins, Solid State Commun. **149**, 1144 (2009).

[43] A. D. Güçlü, P. Potasz, O. Voznyy, M. Korkusinski, and P. Hawrylak, Magnetism and Correlations in Fractionally Filled Degenerate Shells of Graphene Quantum Dots, Phys. Rev. Lett. **103**, 246805 (2009).

[44] J. P. C. Baldwin and Y. Hancock, Effect of random edge-vacancy disorder in zigzag graphene nanoribbons, Phys. Rev. B **94**, 165126 (2016).

[45] M. Raczkowski and F. F. Assaad, Interplay between the edge-state magnetism and long-range coulomb interaction in zigzag graphene nanoribbons: Quantum Monte Carlo study, Phys. Rev. B **96**, 115155 (2017).

[46] M. Sepioni, R. R. Nair, S. Rablen, J. Narayanan, F. Tuna, R. Winpenny, A. K. Geim, and I. V. Grigorieva, Limits on Intrinsic Magnetism in Graphene, Phys. Rev. Lett. **105**, 207205 (2010).

[47] S. Hao, K. Takai, F. Kang, and T. Enoki, Electronic and magnetic properties of acid-adsorbed nanoporous activated carbon fibers, Carbon **46**, 110 (2008).

[48] R. Nair, M. Sepioni, I.-L. Tsai, O. Lehtinen, J. Keinonen, A. Krasheninnikov, T. Thomson, A. Geim, and I. Grigorieva, Spin-half paramagnetism in graphene induced by point defects, Nat. Phys. **8**, 199 (2012).

[49] J. Černák, G. Helgesen, A. T. Skjeltorp, J. Kováč, J. Voltr, and E. Čižmár, Magnetic properties of carbon nanodisk and nanocone powders, Phys. Rev. B **87**, 014434 (2013).

[50] Y. Sun, Y. Zheng, H. Pan, J. Chen, W. Zhang, L. Fu, K. Zhang, N. Tang, and Y. Du, Magnetism of graphene quantum dots, npj Quantum Mater. **2**, 1 (2017).

[51] Y. Sun, Y. Zheng, J. Chen, W. Zhang, N. Tang, and Y. Du, Intrinsic magnetism of monolayer graphene oxide quantum dots, Appl. Phys. Lett. **108**, 033105 (2016).

[52] M. Bonfanti, S. Achilli, and R. Martinazzo, Sticking of atomic hydrogen on graphene, J. Phys.: Condens. Matter **30**, 283002 (2018).

[53] T. Yamamoto, T. Noguchi, and K. Watanabe, Edge-state signature in optical absorption of nanographenes: Tight-binding method and time-dependent density functional theory calculations, Phys. Rev. B **74**, 121409(R) (2006).

[54] M. Ezawa, Metallic graphene nanodisks: Electronic and magnetic properties, Phys. Rev. B **76**, 245415 (2007).

[55] Z. Z. Zhang, K. Chang, and F. M. Peeters, Tuning of energy levels and optical properties of graphene quantum dots, Phys. Rev. B **77**, 235411 (2008).

[56] D. A. Bahamon, A. L. C. Pereira, and P. A. Schulz, Inner and outer edge states in graphene rings: A numerical investigation, Phys. Rev. B **79**, 125414 (2009).

[57] Y. Ominato and M. Koshino, Orbital magnetism of graphene flakes, Phys. Rev. B **87**, 115433 (2013).

[58] A. Ganguly, S. Sharma, P. Papakonstantinou, and J. Hamilton, Probing the thermal deoxygenation of graphene oxide using high-resolution in situ x-ray-based spectroscopies, J. Phys. Chem. C **115**, 17009 (2011).

[59] M. Acik, G. Lee, C. Mattevi, A. Pirkle, R. M. Wallace, M. Chhowalla, K. Cho, and Y. Chabal, The role of oxygen during thermal reduction of graphene oxide studied by infrared absorption spectroscopy, J. Phys. Chem. C **115**, 19761 (2011).

[60] K. M. McCreary, A. G. Swartz, W. Han, J. Fabian, and R. K. Kawakami, Magnetic Moment Formation in Graphene Detected by Scattering of Pure Spin Currents, Phys. Rev. Lett. **109**, 186604 (2012).

[61] S. Sharma, A. M. Rostas, L. Bordonali, N. MacKinnon, S. Weber, and J. G. Korvink, Micro and nano patternable magnetic carbon, J. Appl. Phys. **120**, 235107 (2016).

[62] M. Zhang, X. Wang, H. Sun, N. Wang, Q. Lv, W. Cui, Y. Long, and C. Huang, Enhanced paramagnetism of mesoscopic graphdiyne by doping with nitrogen, Sci. Rep. **7**, 1 (2017).

[63] J. Li, S. Sanz, M. Corso, D. J. Choi, D. Peña, T. Frederiksen, and J. I. Pascual, Single spin localization and manipulation in graphene open-shell nanostructures, Nat. Commun. **10**, 1 (2019).

[64] T. Enoki, Intercalation and guest-host interaction in nano-graphite, J. Phys. Chem. Solids **65**, 103 (2004).

[65] T. Tang, N. Tang, Y. Zheng, X. Wan, Y. Liu, F. Liu, Q. Xu, and Y. Du, Robust magnetic moments on the basal plane of the graphene sheet effectively induced by oh groups, Sci. Rep. **5**, 8448 (2015).

[66] A. V. Krasheninnikov, P. O. Lehtinen, A. S. Foster, P. Pyykkö, and R. M. Nieminen, Embedding Transition-Metal Atoms in Graphene: Structure, Bonding, and Magnetism, Phys. Rev. Lett. **102**, 126807 (2009).

[67] M. P. López-Sancho, F. de Juan, and M. A. H. Vozmediano, Magnetic moments in the presence of topological defects in graphene, Phys. Rev. B **79**, 075413 (2009).

[68] B. Wang and S. T. Pantelides, Magnetic moment of a single vacancy in graphene and semiconducting nanoribbons, Phys. Rev. B **86**, 165438 (2012).

[69] F. Yndurain, Effect of hole doping on the magnetism of point defects in graphene: A theoretical study, Phys. Rev. B **90**, 245420 (2014).

[70] J. Akola, H. P. Heiskanen, and M. Manninen, Edge-dependent selection rules in magic triangular graphene flakes, Phys. Rev. B **77**, 193410 (2008).

[71] S. Reich, J. Maultzsch, C. Thomsen, and P. Ordejon, Tight-binding description of graphene, Phys. Rev. B **66**, 035412 (2002).

[72] E. H. Lieb, Two Theorems on the Hubbard Model, Phys. Rev. Lett. **62**, 1201 (1989).